Available online at https://link.springer.com/journal/42241
http://www.jhydrodynamics.com
Journal of Hydrodynamics, 2023, 35(2): 287-298
https://doi.org/10.1007/s42241-023-0020-4

Simulation of open channel flows by an explicit incompressible mesh-free method

Zhi-jian Huang[1], Ti-bing Xu[1*], David Z. Zhu[1, 2], Song-da Zhang[3]
1. *School of Civil and Environmental Engineering and Geography Science, Ningbo University, Ningbo 315211, China*
2. *Department of Civil and Environmental Engineering, University of Alberta, Alberta, Canada*
3. *Ningbo River Management Center, Ningbo 315303, China*

(Received August 16, 2022, Revised November 9, 2022, Accepted December 8, 2022, Published online May 4, 2023)

Abstract: In this study, to simulate open channel flows, an explicit incompressible mesh-free method is employed in which the pressure field is obtained by explicitly solving the pressure Poisson equation. To capture the velocity information in open channel flows, the source term in the pressure Poisson equation is modified while the spatial discretization of gradient and Laplacian models is based on the moving particle semi-implicit (MPS) method. The inflow boundary condition is treated by injecting fluid particles into the domain according to the inlet discharge, and the outflow condition is handled by prescribing the pressure distribution and removing the fluid particles beyond the domain. The explicit incompressible mesh-free method is then used to simulate open channel flows, including weir flow, hydraulic jump, and flow over an obstacle. In the simulations, velocity distribution and flow pattern are examined. The simulated results are compared to available experimental measurements and other numerical results. There is a good agreement between the simulated results and the experimental measurements. It shows that the explicit incompressible mesh-free method can reproduce the flow characteristics in the open channel flows.

Key words: Mesh-free method, explicit scheme, weir flow, hydraulic jump, velocity distribution

0. Introduction

The mesh-free methods including the smoothed particle hydrodynamics (SPH)[1-2] and moving particle semi-implicit (MPS) method[3-6] represent fluid by a set of discretized movable points/particles. Wen et al.[7] developed a multiphase MPS method to simulate bubbly flows with complex interfaces and found that the numerical results are in good agreement with the experimental results. Lyu and Sun[8] developed an enhanced particle shifting technique in SPH to improve the calculation of the free surface, and more uniform particle distribution in the vicinity of the free surface can be achieved. Zhang et al.[9] coupled the smoothed finite element method with SPH to simulate liquid sloshing with rigid and deformable structures, and the coupled method can obtain more accurate results. Khayyer et al.[10] simulated the hydroelastic fluid-structure interaction by using an enhanced multi-resolution solver with incompressible SPH (ISPH) and SPH. The improved techniques make the mesh-free method robust and capable of handling more engineering problems[11-13].

In the mesh-free methods, there are several approaches for calculating the pressure field when simulating hydrodynamics. The first approach is to obtain the pressure by using an equation of state, referred to as the weakly-compressible scheme[14-16]. This scheme is an explicit scheme, and the pressure field is calculated by a direct relationship. In the scheme, the incompressible fluid is usually assumed to be weakly compressible and a parameter of artificial sound speed is used to control compressibility to less than 1%. The second approach is an implicit scheme by solving the pressure Poisson equation by iteration to obtain the pressure field[17-19]. The implicit scheme usually involves solving a matrix equation each time step. The MPS method and ISPH method both belong to the implicit scheme in terms of pressure field calculation.

As the third approach, the pressure Poisson equation is explicitly solved with approximation equations when modeling incompressible fluid flow. This explicit mesh-free scheme has been developed and applied to solve hydrodynamic problems[20-21]. Based

Biography: Zhi-jian Huang (1998-), Male, Master,
E-mail: hzj930128@163.com
Corresponding author: Ti-bing Xu,
E-mail: xu320@uregina.ca

on the SPH algorithm, Xu[22] proposed an explicit scheme to calculate the pressure Poisson equation in the framework of the MPS method. Ye et al.[23] employed an MPS explicit solver for the pressure Poisson equation to simulate dam-break flows under different downstream conditions. They showed that the explicit solver can obtain the free surface profiles in agreement with experimental observations, and the calculated pressure field is smooth. Zuo et al.[24] employed the MPS explicit solver to simulate dam-break flow, and impact pressure by the dam-break wave can be reflected agreeing well with the experimental measurements. Xiao and Jin[25] developed an explicit scheme to solve the pressure Poisson equation in which an equation of state is used to calculate the pressure in the next time step in the explicit scheme.

In the MPS explicit solver for the pressure Poisson equation, an approximation is incorporated by replacing the pressure field in the next time step with that of the previous time step[22-24]. However, there is a discrepancy due to the approximation in calculating the pressure field. This raises the question that this approximation could affect simulation results, especially when applying the scheme to simulate open channel flows which usually require a considerable running time from the initial condition. To address this issue, this study aims to evaluate the MPS explicit solver in simulating a series of open channel flows including weir flow, hydraulic jump, and flow over an obstacle. To simulate the flows, the source term in solving the pressure Poisson equation is modified compared with the previous studies[22-24] aiming to improve its accuracy. To account for open boundary conditions in open channel flows, the inflow boundary condition is treated by injecting fluid particles into the domain according to discharge (velocity and water height at the inlet). The outflow condition is handled by prescribing hydrostatic pressure to fluid particles and removing them when they move beyond the boundary. In the simulations, the particle distance in the explicit mesh-free method is examined and the velocity distributions in the three types of open channel flows are investigated.

1. Explicit incompressible mesh-free method

In this section, the following contents are presented, including the governing equations, spatial operators, time-splitting scheme, and boundary conditions.

1.1 *Governing equations*

The governing equations for incompressible fluid flow include mass conservation and momentum equations. They are expressed in the Lagrangian framework as:

$$\frac{1}{\rho}\frac{\mathrm{D}\rho}{\mathrm{D}t} = \nabla \cdot \boldsymbol{u} = 0 \tag{1}$$

$$\frac{\mathrm{D}\boldsymbol{u}}{\mathrm{D}t} = -\frac{1}{\rho}\nabla p + \nu \nabla^2 \boldsymbol{u} + + \frac{1}{\rho}\nabla \cdot \boldsymbol{\tau} \tag{2}$$

where ρ is the density, t is the time, $\boldsymbol{u}$ is the velocity vector, p is the pressure, ν is the laminar kinematic viscosity, $\boldsymbol{g}$ is the gravity force, $\boldsymbol{\tau}$ is the turbulence stress tensor which is calculated according to the sub particle scale (SPS) model.

To calculate the stress tensor $\boldsymbol{\tau}$, large eddy simulation (LES)[23, 26] is adopted. In LES, eddies can be resolved by the computational grid in the mesh-based method and particle distance in the mesh-free method[27]. In the particle distance scale, it is referred to as the SPS model, in which the turbulence eddy viscosity is introduced as ν_t. The SPS turbulence stress is expressed as

$$\tau_{ab} = 2\nu_t S_{ab} - \frac{2}{3}k\delta_{ab} \tag{3}$$

where δ_{ab} is the Kronecker operator, S_{ab} is the strain rate, k is the turbulence kinetic energy and a, b are the coordinate directions.

The turbulence eddy viscosity[23, 26] is calculated as

$$\nu_t = (C_s \Delta l)^2 |S| \tag{4}$$

where C_s is the Smagorinsky constant, $C_s = 0.2$ in this study, Δl is the particle distance in the mesh-free method and $|S|$ is the local strain rate.

1.2 *MPS spatial operators*

As a Lagrangian method, the MPS method discretizes the fluid and solid boundaries into a set of movable particles. They have flow properties such as velocity $\boldsymbol{u}$ and pressure p, while their positions $(\boldsymbol{r})$ are updated at each time step. In the calculation, a weighting function is used to relate the separated particles to weigh the contributions between particles. The weighting function in this study is expressed as follows:

$$w_{ij} = \left(1 - \frac{r_{ij}}{r_e}\right)^3, \quad r_{ij} \le r_e \tag{5a}$$

$$w_{ij} = 0, \quad r_{ij} > r_e \tag{5b}$$

where i, j are the indexes of particles, r_{ij} is the distance between particles i, j, r_e is the interaction radius for the weighting function which is usually several times the initial particle distance Δl, and in this study, $r_e = 4.0\Delta l$. By using this interaction radius, the MPS method can obtain good results according to the previous studies[5, 19, 22-24, 28].

The sum of the weighting function values is defined as the particle number density[3]

$$n_i = \sum_{j \neq i} w_{ij} \tag{6}$$

where i is the target particle, j is the neighboring particle. In the initial condition, the particle number density is n_0 which keeps constant throughout the entire calculation.

Based on the weighting function, the gradient model that discretizes the pressure gradient term in the governing equations is expressed as[3]

$$\langle \nabla \phi \rangle_i = \frac{D_m}{n_0} \sum_{j \neq i} \frac{\phi_j - \phi_i}{r_{ij}^2} \boldsymbol{r_{ij}} w_{ij} \tag{7}$$

where D_m is the dimension coefficient, ϕ is a scalar and $\boldsymbol{r}_{ij}$ is the position vector.

When applying the gradient model, Eq. (7), to calculate the pressure gradient term, the minimum value of the pressure in the interaction circle for the target particle is used to generate the repulsive force[3]. It is expressed as

$$\langle \nabla p \rangle_i = \frac{D_m}{n_0} \sum_{j \neq i} \frac{p_j - p_{i,\min}}{r_{ij}^2} \boldsymbol{r_{ij}} w_{ij} \tag{8}$$

where $p_{i,\min}$ is the minimum value of the pressure in the interaction circle for the target particle i.

The Laplacian model by Xu and Jin[28-29] is used in this study:

$$\langle \nabla^2 \phi \rangle_i = \frac{D_m}{n_0} \sum_{j \neq i} \frac{\phi_j - \phi_i}{r_{ij}^2} G_{ij} \tag{9}$$

$$G_{ij} = (3D_m - 2) w_{ij} + r_{ij} \frac{\partial w_{ij}}{\partial r_{ij}} \tag{10}$$

According to this Laplacian model, an explicit model to calculate the pressure field is proposed and applied to simulate hydrodynamic problems[22-24]. In the model, the pressure is calculated as

$$p_i^{k+1} = \frac{D_m \sum_{j \neq i} p_j^k \frac{G_{ij}^*}{(r_{ij}^*)^2} - \frac{\rho}{\Delta t} \left(\frac{\mathrm{D}n}{\mathrm{D}t} \right)_i^*}{D_m \sum_{j \neq i} \frac{G_{ij}^*}{(r_{ij}^*)^2}} \tag{11}$$

In the model, the source term in Eq. (11) is based on the incompressible condition of density variation equal to zero, and it is named as the incompressible explicit model with the previous source term.

1.3 *Improved explicit pressure calculation*

A predictor-corrector time-splitting scheme is used to solve the governing equations. The viscous, gravity, and turbulence stress tensor terms are calculated in the predictor to obtain intermediate flow properties including intermediate particle position $\boldsymbol{r}^*$ and intermediate velocity $\boldsymbol{u}^*$:

$$\boldsymbol{u}^* = \boldsymbol{u}^k + \Delta t \left(\nu \nabla^2 \boldsymbol{u}^k + \boldsymbol{g} + \frac{1}{\rho} \nabla \cdot \boldsymbol{\tau}^k \right) \tag{12}$$

$$\boldsymbol{r}^* = \boldsymbol{r}^k + \boldsymbol{u}^* \Delta t \tag{13}$$

where the superscript $*$ denotes the intermediate flow properties, k is the previous time step and Δt is the time step length.

In the corrector, the pressure gradient term is solved using the pressure gradient model and the particles' positions are updated correspondingly:

$$\boldsymbol{u}^{k+1} = \boldsymbol{u}^* - \Delta t \frac{1}{\rho} \nabla p^{k+1} \tag{14}$$

$$\boldsymbol{r}^{k+1} = \boldsymbol{r}^k + \boldsymbol{u}^{k+1} \Delta t \tag{15}$$

where $k+1$ represents the new time step.

According to Eqs. (1), (13), the following equation can be obtained

$$\langle \nabla^2 p \rangle_i^{k+1} = \frac{\rho}{\Delta t} \langle \nabla \cdot \boldsymbol{u}^* \rangle_i \tag{16}$$

According to the Laplacian model, Eqs. (9), (10), an explicit relationship between pressure and the known flow properties can be established as

$$p_i^{k+1} = \frac{D_m \sum_{j \neq i} \frac{p_j^k G_{ij}^*}{(r_{ij}^*)^2} - S_{ci}}{D_m \sum_{j \neq i} \frac{G_{ij}^*}{(r_{ij}^*)^2}} \tag{17}$$

The source term S_{ci} in Eq. (17) can be expressed in a different form from the incompressible condition, either velocity divergence-free condition or density variation equal to zero. This study employs a mixed form of velocity divergence-free and density variation equal to zero. This is different from previous studies[22-24] by using the explicit scheme and it can improve the accuracy of velocity calculation in open channels. The mixed source term is expressed as:

$$S_{ci} = 0.5\frac{\rho n_0}{(\Delta t)^2}\frac{n_i^* - n_0}{n_0} + 0.5\frac{\rho}{\Delta t}\left(\frac{\mathrm{D}n}{\mathrm{D}t}\right)_i^*, \quad n_i^* > n_0 \quad (18a)$$

$$S_{ci} = \frac{\rho}{n_0 \Delta t}\left(\frac{\mathrm{D}n}{\mathrm{D}t}\right)_i^*, \quad n_i^* > \beta n_0, \quad n_0 > n_i^* \quad (18b)$$

By using the mixed source term to calculate the pressure field, it is found that using the value 0.5 as half the velocity divergence-free condition and half density variation equal to zero condition can obtain good velocity distribution in the open channel flows.

During particles' position updating, particles can approach each other, and when two particles' distance is less than $0.95\Delta l$, a collision is activated to repel the two approaching particles, avoiding particle clustering. This collision can be referred to as in the previous studies by the mesh-free method[28]. The collision distance $0.95\Delta l$ is used which is based on the previous studies using the collision model, and this parameter can obtain good numerical results [5, 19, 22-24]. It should be noted that the particle shifting technique can also be used to solve the particle clustering in the mesh-free method [8, 13, 17].

Equation (17) establishes the pressure calculation for the mesh-free method. There are two features of this scheme: (1) The pressure field is calculated explicitly using the flow information from the previous and intermediate time steps, (2) The incompressibility condition can be satisfied for the incompressible fluid flow. On the other hand, in the explicit scheme, there is a discrepancy in using the flow information from the previous time step to replace the flow properties in the next time step. To minimize this approximate discrepancy, the time step should be small, and in this study, the Courant-Friedrichs-Lewy (CFL) condition is implemented [22, 24]

$$\Delta t < 0.25 \min\left\{\frac{\Delta l}{U_{\max}}, \frac{(\Delta l)^2}{\nu}, \sqrt{\frac{\Delta l}{|g|}}\right\} \quad (19)$$

1.4. *Boundary conditions*

In the mesh-free method, the fluid and the boundary are discretized into a set of particles with the same initial distance Δl, and four layers of ghost particles are set beyond the solid particles due to the lack of particles in the vicinity of the boundary[3, 5, 26, 30]. Velocities of the solid particles and ghost particles are set to satisfy the non-slip condition. Pressure for the solid particles is calculated by Eq. (17) and their ghost particles are assigned the same pressure as the solid particles.

For the free surface condition, the intermediate particle number density is used for identification[3]. It is expressed as

$$n_i^* < \beta n_0 \quad (20)$$

where the coefficient $\beta = 0.98$. When Eq. (20) is satisfied, the identified particle i is on the free surface with prescribing zero pressure.

To simulate open channel flows, open boundary conditions with the inflow and outflow are required. To account for the inflow boundary condition, fluid particles are injected into the simulation domain with prescribing velocity. The velocity and height of the injected fluid particles are set according to the discharge to the channel. The length of the inflow zone is equal to the interaction radius for the weighting function r_e and this can ensure that there are sufficient particles in the vicinity of the inlet. The velocity for the fluid particles in the inflow zone is all equal to the injected velocity and this setting can satisfy the continuity equation. An outflow zone equal to the length of the interaction radius r_e is also set in which the fluid particles are assigned to the hydrostatic pressure distribution and their velocity is calculated according to the momentum equation. At the end of the outflow zone, the fluid particles are removed from the domain. The setting for the open boundary conditions is shown in Fig. 1. A similar boundary condition was also used in the previous studies[16, 31].

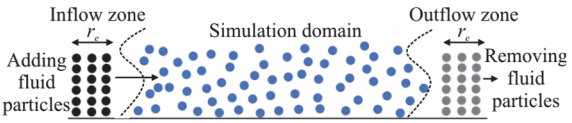

Fig. 1 (Color online) Open boundary conditions to simulate open channel flows

2. Simulation of weir flows

In this section, the mesh-free method is validated by simulating weir flows, in which the simulated velocity distributions are compared to available experimental observations.

The experiments by Kirkgoz et al.[32] on the weir flows were conducted in a horizontal channel of 2.4 m

in length, 0.2 m in width, and 0.2 m in depth, in which a rectangular broad-crested weir and a triangular broad-crested weir were respectively equipped, and their geometries are shown in Fig. 2. In the experiments, they measured velocity distributions at the vertical sections $x = 0.905$ m, 0.995 m for the rectangular broad-crested weir flow, and vertical sections $x = 0.960$ m, 1.066 m for the triangular broad-crested weir. For the rectangular broad-crested weir flow, the inlet water height is $H = 0.130\,\mathrm{m}$ and the inflow velocity is $V = 0.0866\,\mathrm{m/s}$ according to the experiments, which

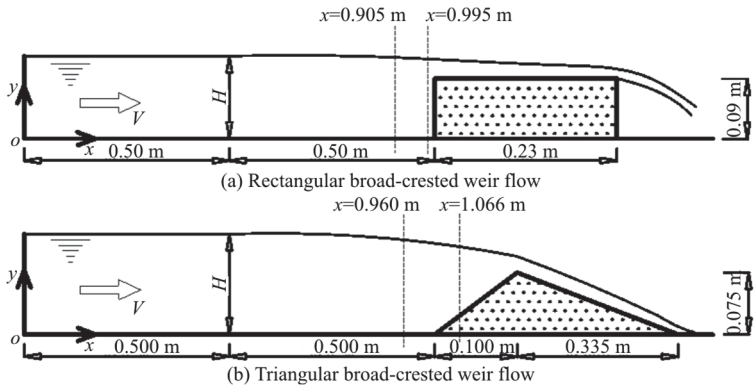

Fig. 2 The geometry of the weir flows in the simulation by the mesh-free method

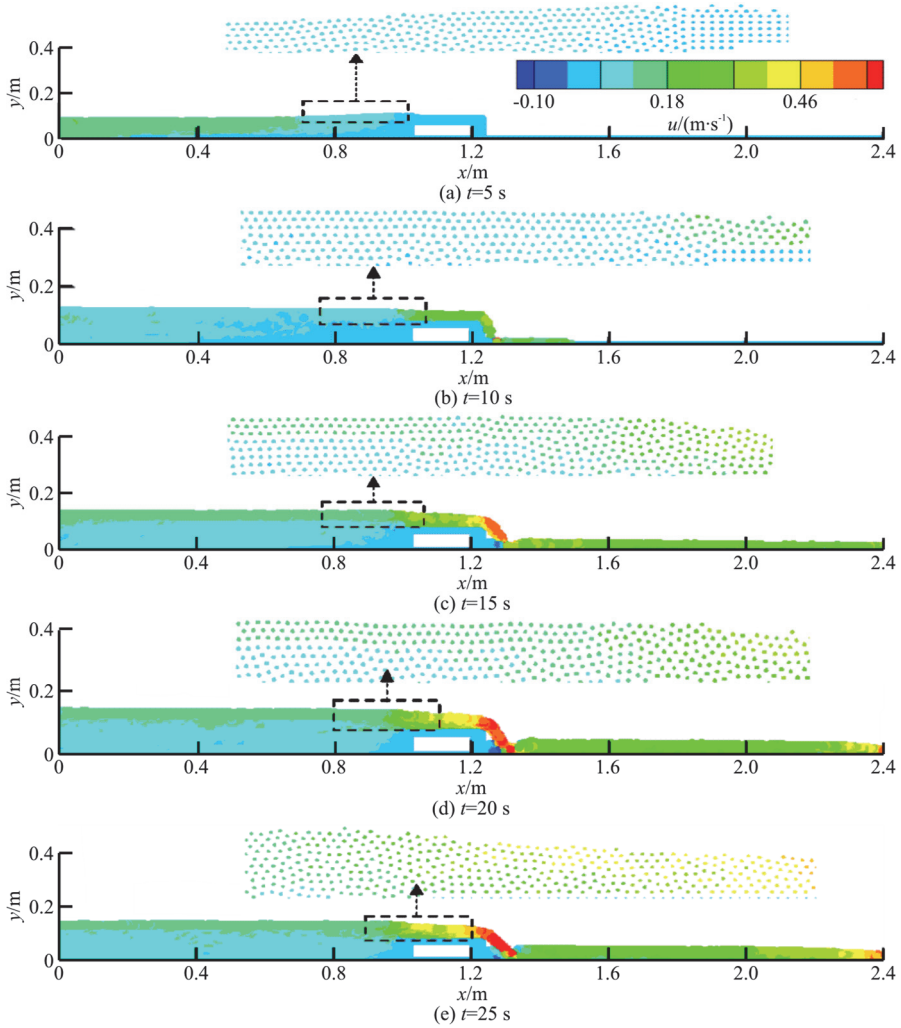

Fig. 3 (Color online) Simulated horizontal velocity field for the rectangular broad-crested weir flow at different time steps (the particle distance in the simulation by the explicit mesh-free method $\Delta l = 0.005$ m)

are used at the inlet for the inflow boundary condition. For the triangular broad-crested weir flow, the water height is $H = 0.105\,\mathrm{m}$ and the inflow velocity is $V = 0.0952\,\mathrm{m/s}$ in the experiments which are also used in the boundary treatment by prescribing the velocity for the injected fluid particles.

The mesh-free method is applied to simulate the two weir flows and the simulations were carried out in 2-D as the flow mainly shows to be 2-D. In the simulation of the rectangular broad-crested weir flow, three different particle distances of $\Delta l = 0.004$ m, 0.005 m and 0.010 m are implemented to examine the sensitivity of the particle distance.

Figure 3 shows the horizontal velocity field of the rectangular broad crested weir flow at different times simulated by the particle distance $\Delta l = 0.005$ m in the mesh-free method. The simulation was conducted in an empty channel by injecting fluid particles according to the open boundary condition explained in Section 1.4. It can be observed that the channel is gradually filled with fluid particles and the flow gradually reaches a steady state. From $t = 5$ s, the water flows over the weir, forming a jet with a high velocity which is obvious at $t = 15$ s, 20 s and 25 s. From $t = 20$ s to 25 s, the weir flow shows less variation in terms of the velocity field and water level, especially before the weir. In the figure, a detailed view is shown to illustrate the particle distribution and uniform particle distribution can be observed.

Figure 4 shows the horizontal velocity profiles for the rectangular broad-crested weir flow at the vertical sections $x = 0.905$ m, 0.995 m, including the simulated results by different source terms, and experimental and numerical results by Kirkgoz et al.[32]. In Fig. 4(a), it can be seen that the horizontal velocity distributions of the three results by using different particle distances are in a similar trend to the experimental measurements. By refining the particle distances to $\Delta l = 0.005$ m, the velocity near the bottom can agree with the experimental results better. The velocity distribution at $x = 0.995$ m is well reproduced by the mesh-free method for all three particle distances ($\Delta l = 0.010$ m, 0.004 m and 0.005 m), as shown in Fig. 4(b). The numerical results by using different source terms in the explicit model (respectively as Eqs. (11), (17)) are also shown in Fig. 4. Using the mixed source term as Eq. (17) can calculate more accurate velocity, which is obvious in Fig. 4(a). This comparison of the velocity at the two sections suggests that the mesh-free method by using the explicit scheme can calculate the velocity field, reflecting the velocity distribution in the weir flow.

The mesh-free method is then applied to simulate the triangular broad-crested weir flow by using the particle distance $\Delta l = 0.005$ m. The inflow and outflow boundary conditions are set according to the open boundary conditions explained in Section 1.4. The simulated velocity profiles at two vertical sections $x = 0.960$ m, 1.066 m are shown in Fig. 5. The experimental measurements by Kirkgoz et al.[32] and their numerical results are also included in the figure. It can be seen from the figures that the velocity at the two sections is reproduced by the explicit mesh-free method. There are also some discrepancies in the velocity comparison at the two sections, especially for the velocity close to the bottom. This could be caused by the boundary condition used in the numerical scheme. There is a particle number density deficiency in the vicinity of the solid boundary as the interaction circle defined by the weighting function is partially filled with particles. Although in the boundary treatment, ghost particles are used to offset the particle number deficiency, the accuracy to calculate the velocity is affected when solving the pressure Poisson equation explicitly by using Eq. (17).

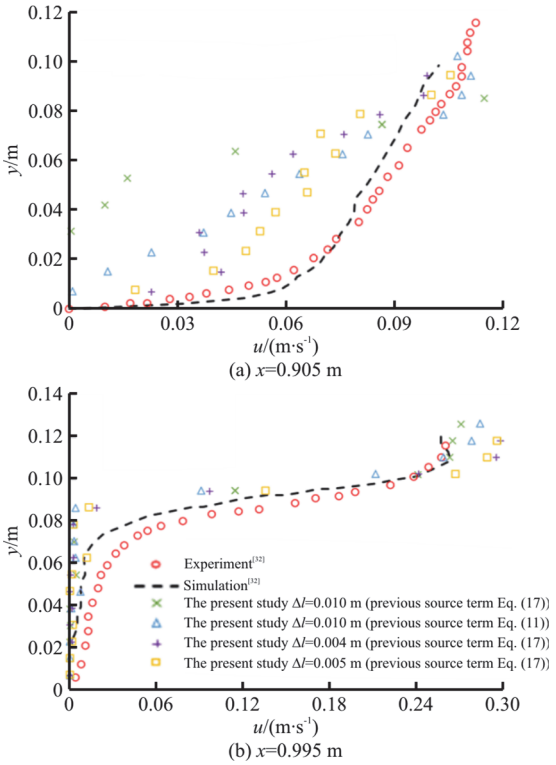

Fig. 4 (Color online) Horizontal velocity profiles for the rectangular broad-crested weir flow, including the simulated results by different source terms (Eqs. (11), (17)), experimental and numerical results by Kirkgoz et al.[32]

3. Simulation of hydraulic jump

The mesh-free method is validated by simulating another type of open channel flow: hydraulic jump, which is a problem with large deformation for the free

surface and intense turbulence. The simulated velocity is compared with available experimental observations.

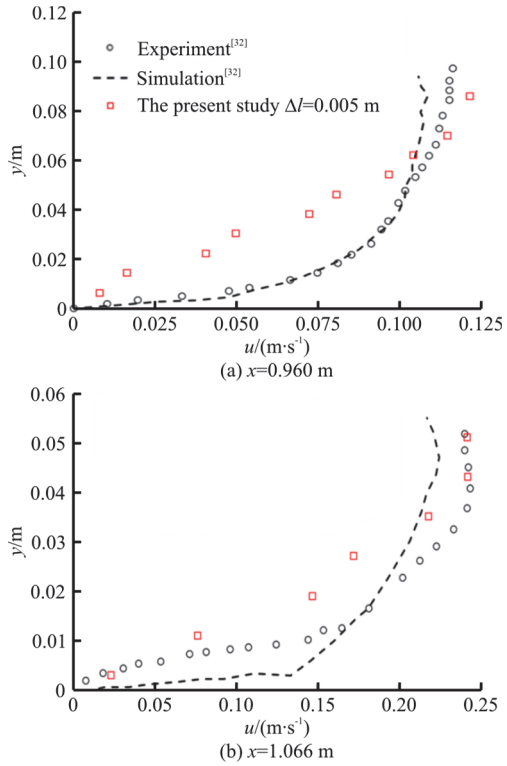

Fig. 5 (Color online) Horizontal velocity profiles for the triangular broad-crested weir flow, including the present numerical results, experimental and numerical results by Kirkgoz et al.[32]

The experiments for the hydraulic jump by Xin[33] were conducted in a horizontal channel of 11.6 m in length, 0.3 m in width, and 0.5 m in depth. The velocity distribution was measured by laser Doppler anemometer (LDA) at several different vertical sections in the channel for the hydraulic jump with different Froude numbers. In the present study, the hydraulic jump is simulated by the explicit mesh-free method, and the diagram of the numerical setup for the flow is shown in Fig. 6. The simulation is conducted in 2-D. In the initial condition, the computational domain is empty, by setting the inlet water depth $h = 0.09$ m and the inlet velocity $V = 2.0$ m / s. With this inflow boundary condition by periodically injecting fluid particles into the domain, the computational domain can gradually be filled with fluid particles, reaching a steady state. The outflow condition is prescribed as that the fluid particles enter the outflow zone with the hydrostatic pressure distribution. The fluid particles leaving the end of the domain are removed in the boundary treatment. To examine the sensitivity of the particle distance in the mesh-free method, three particle distances ($\Delta l = 0.018$ m, 0.005 m and 0.010 m) are implemented to simulate the hydraulic jump.

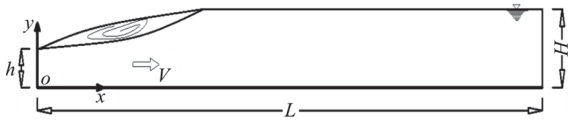

Fig. 6 The numerical setup for the hydraulic jump

Figure 7 shows the simulated horizontal velocity field for the hydraulic jump with the Froude number $Fr = 2.1$ $(Fr = V/(gh)^{1/2})$ at different time steps by the particle distance $\Delta l = 0.010$ m. In the figure, the developing process for the hydraulic jump can be observed, which shows less variation in the flow pattern from $t = 15$ s. This hydraulic jump is characterized by a bottom jet, showing a high-velocity field. The jet becomes shorter with the increase of the water level, and maintains an almost constant length from $t = 15$ s to 25 s. The rolling free surface in the hydraulic jump is also captured by the mesh-free method, showing a negative horizontal velocity in the figure. The particle distribution is shown in the detailed view for the flow in the figure and the distribution is uniform.

To show the mesh-free method in reproducing the flow characteristics in the hydraulic jump, the simulated velocity profiles at different vertical sections $x = 1.41$ m, 1.87 m, 2.31 m and 2.80 m are compared with the experimental measurements by Xin[33] and the numerical results by Liu and Drewes[34], shown in Fig. 8. The present simulation results by different particle distances are shown in the figure to demonstrate the sensitivity of the particle distance. The velocity variation trend is generally reproduced by the explicit mesh-free method. There are some discrepancies in the velocity comparison at vertical sections $x = 1.41$ m, 1.87 m. The discrepancies become smaller at vertical sections $x = 2.31$ m, 2.80 m, agreeing better with the experimental measurements at these two sections. All three particle distances can simulate similar velocity profiles in the hydraulic jump, suggesting that there is a good numerical convergence in terms of the particle distance.

To further illustrate the explicit mesh-free method in capturing the flow properties, it is applied to simulate a hydraulic jump with another Froude number $Fr = 4.4$. To simulate the hydraulic jump, the particle distance $\Delta l = 0.010$ m is used and the inflow velocity and water depth used in the inflow boundary condition are respectively $V = 3.1$ m / s and $h = 0.05$ m. The tailwater depth in the hydraulic jump is set with $H = 0.267$ m for the outflow boundary by defining the fluid particles in the outflow zone as the hydrostatic pressure distribution. The simulated velo-

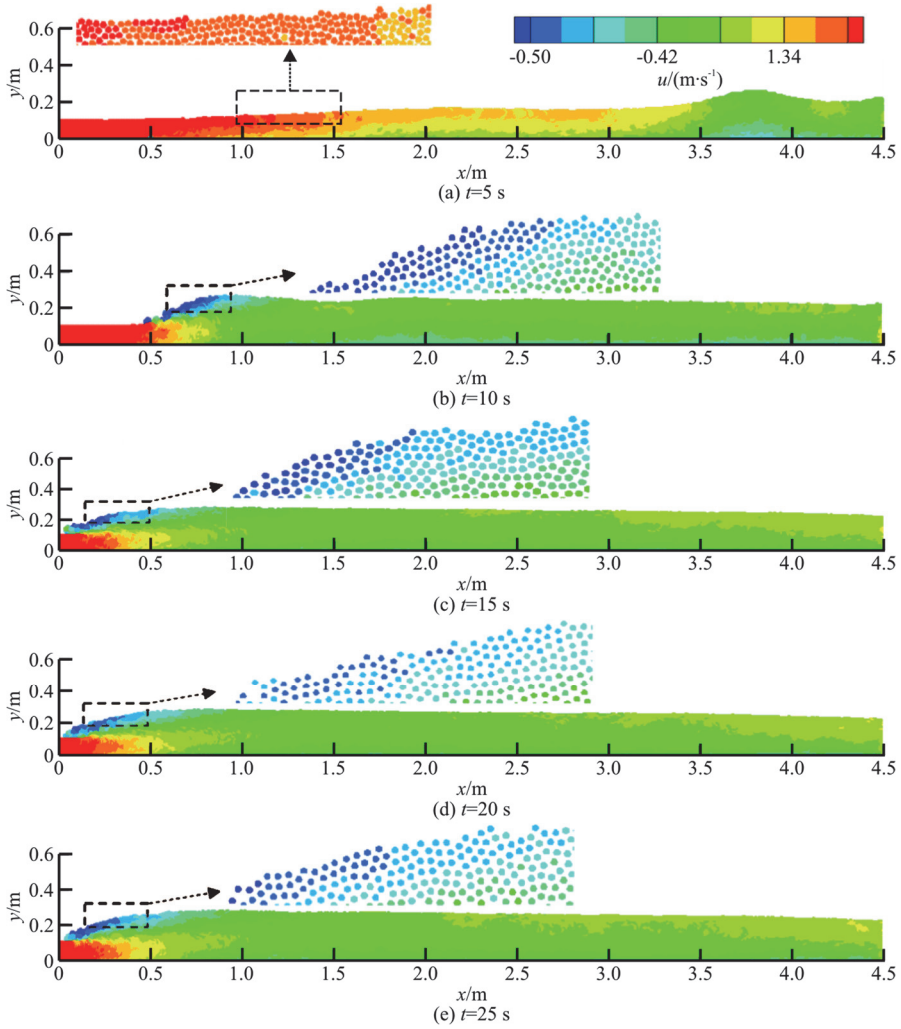

Fig. 7 (Color online) Simulated horizontal velocity field for the hydraulic jump with the Froude number $Fr = 2.1$ at different time steps by the explicit mesh-free method

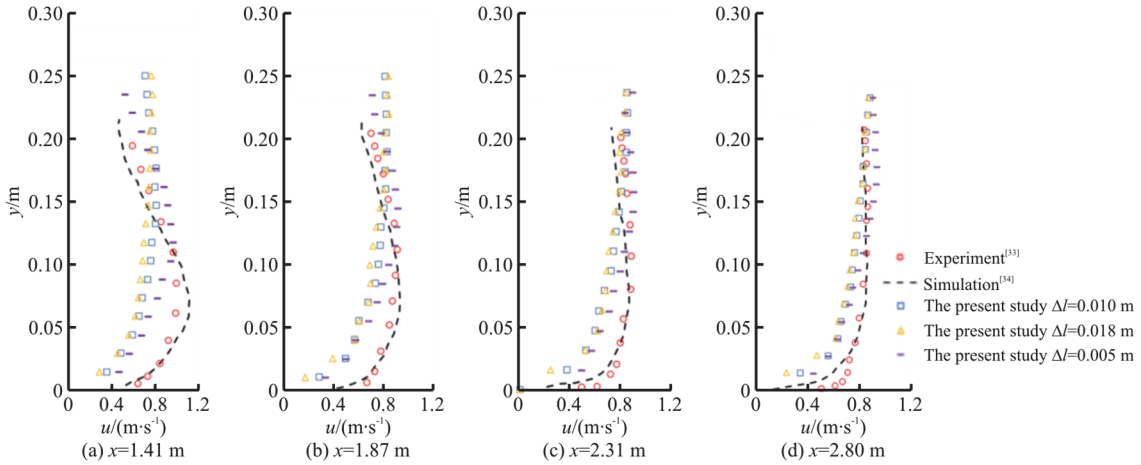

Fig. 8 (Color online) Horizontal velocity in the hydraulic jump with Froude number $Fr = 2.1$ at different vertical sections

city distribution by the explicit mesh-free method is also compared with the experimental results of Xin[33] and the numerical results of Liu and Drewes[34], shown in Fig. 9. The simulated velocity in the hydraulic jump agrees well with the experimental measurements at all three vertical sections.

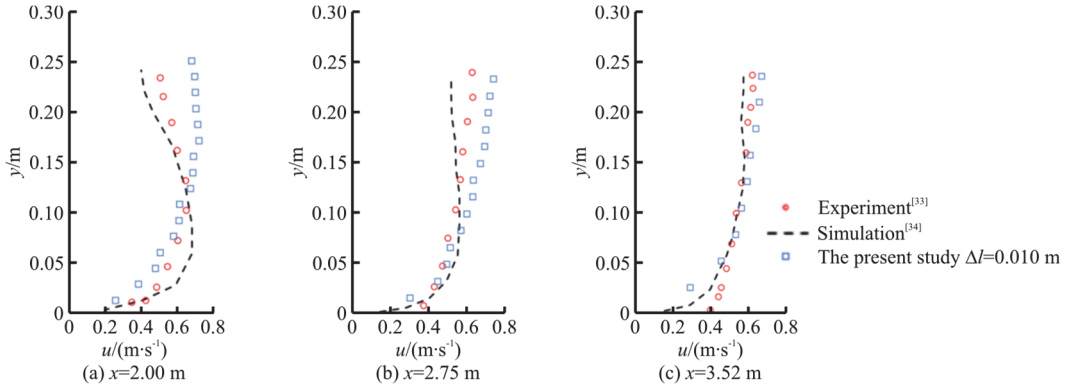

Fig. 9 (Color online) Simulated horizontal velocity distribution for the hydraulic jump with the Froude number $Fr = 4.4$ by the explicit mesh-free method at different vertical sections

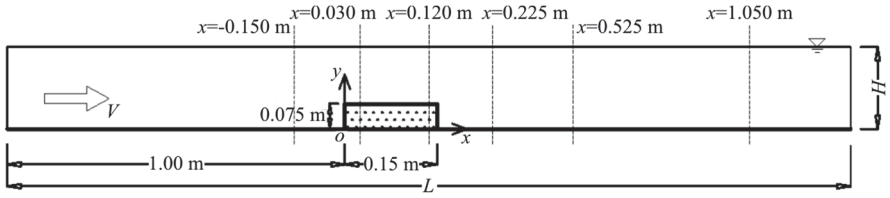

Fig. 10 The numerical setup for the open channel flow over an obstacle

4. Simulation of flow over an obstacle

The third case to validate the mesh-free method is an open channel flow over an obstacle and the numerical setup for the flow is shown in Fig. 10. The experiments were conducted by Leu et al.[35] in a recirculating water tank of 6.0 m long, 0.3 m wide, and 0.4 m high. The velocity distribution at different sections of the flow field over the obstacle was measured using an acoustic Doppler velocimeter (ADV). An obstacle is placed at the bottom of the channel away from the inlet at a distance of 1.0 m. To simulate this flow, the fluid particles are injected from the inlet with a velocity of $V = 0.206$ m / s and water depth $H = 0.245$ m. At the end of the channel, the outflow zone is set and the fluid particles in this zone are prescribed with the hydrostatic pressure. The simulation was conducted in 2-D and the particle distance $\Delta l = 0.005$ m is used. The velocity distribution at the vertical sections $x = -0.150$ m, 0.030 m, 0.120 m, 0.225 m, 0.525 m and 1.050 m measured by Leu et al.[35] is used to compare with the simulation results by the explicit mesh-free method. This flow is also simulated by Fu and Jin[31] and in their simulation, a weakly-compressible mesh-free scheme is used, which calculates the pressure field by an equation of state assuming the incompressible fluid to be weakly compressible.

Figure 11 shows the simulated flow pattern (horizontal velocity field) by the explicit mesh-free method for the open channel flow over an obstacle at different time steps by the particle distance $\Delta l = 0.005$ m. From the figure, the flow is initially from an empty channel and the water level is gradually increasing to a constant level. At $t = 4$ s, the water over the obstacle is characterized by high velocity below the obstacle. To $t = 12$ s, 16 s, the water level in the channel shows very limited variation. In the upstream and downstream of the obstacle, there are some negative horizontal velocity fields close to the bottom.

To show the velocity distribution, Fig. 12 shows the comparison of the horizontal velocity u at different vertical sections (as shown in Fig. 10) in the flow, including the simulation results by the present mesh-free method, the experimental measurements by Leu et al.[35], and the numerical results by Fu and Jin[31]. Generally, the velocity distribution at the six sections is reproduced by the explicit mesh-free method. In some sections such as the vertical section $x = -0.150$ m, 0.225 m and 0.525 m, the simulated velocity is much closer to the velocity trend in the experimental measurements, compared to the numerical results by Fu and Jin[31]. Both the simulated results of this study and by Fu and Jin[31] show negative velocities in the flow field near the bottom of the channel at the vertical section $x = 0.225$ m. Close to the free surface, the simulation results of the present study are more accurate at the vertical section $x = -0.150$ m, 0.225 m, compared to the numerical results by Fu and Jin[31].

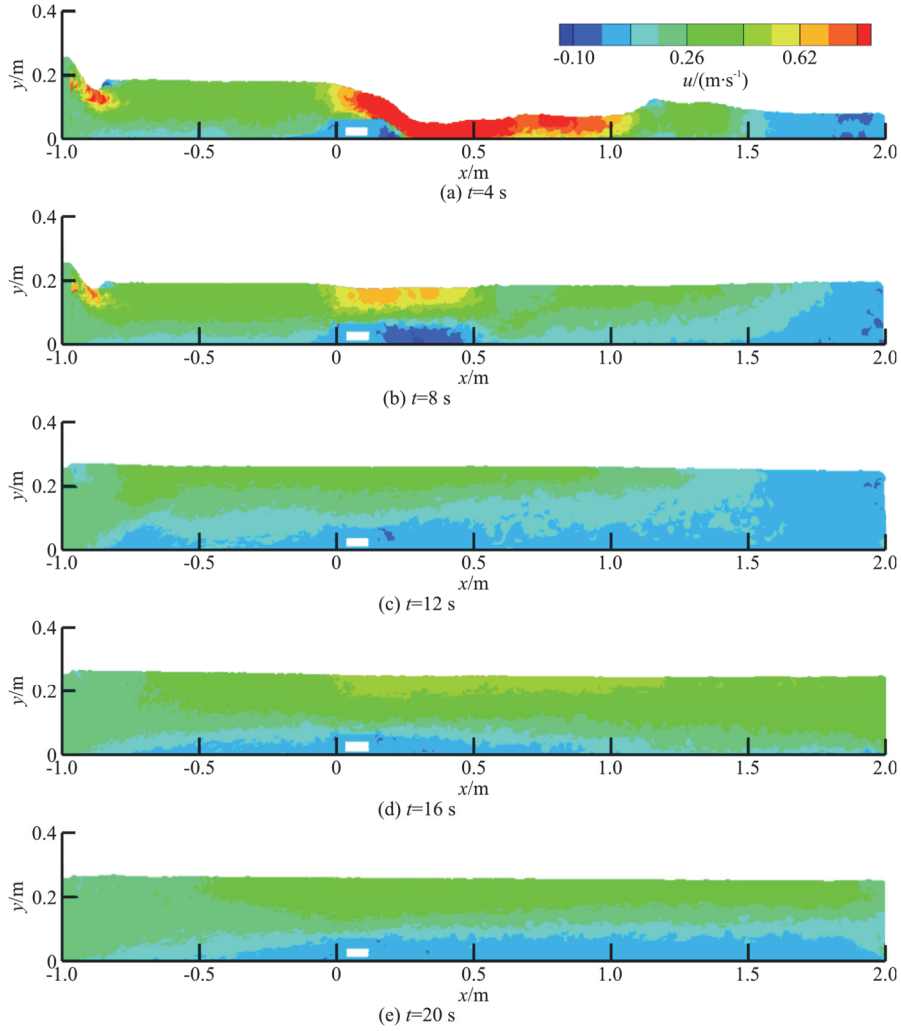

Fig. 11 (Color online) Simulated horizontal velocity pattern for the open channel flow over an obstacle at different time steps by the explicit mesh-free method

5. Conclusions

In this study, an explicit mesh-free method based on the MPS method is employed to simulate the open channel flows. In the explicit method, the pressure Poisson equation is solved, and a mixed source term is used to obtain the velocity information in the open channel flows. In the simulation, the inflow is modeled by setting an inflow zone with the length of interaction radius of the weighting function and the fluid particles in the zone are injected by prescribing the inlet velocity with a water depth according to discharge. An outflow zone with the same length is also set up and the fluid particles entering this zone are assigned to the hydrostatic pressure. The fluid particles are removed from the domain when they leave the end of the outflow zone. The LES-SPS turbulence model is implemented in the method to account for turbulence.

The explicit mesh-free method is validated by three types of open channel flows including the weir flow, hydraulic jump, and flow over an obstacle. In simulating the weir flow, the broad-crested weir flow and triangle-crested weir flow are investigated. The simulated velocity distribution is compared well with the experimental measurements at the vertical sections for the two weir flows. The simulation by using different particle distances in the broad-crested weir flow can obtain similar numerical results, suggesting that there is a good numerical convergence for the numerical method. In the simulation of the hydraulic jump, two Froude numbers, $Fr = 2.1$, 4.4, are considered and the simulated velocity distribution is in good agreement with the experimental measurements at the vertical sections. Different particle distances can simulate similar velocity profiles for the hydraulic jump at $Fr = 2.1$. An open channel flow over an obstacle is also simulated by the explicit mesh-free method. The velocity simulated by the present method

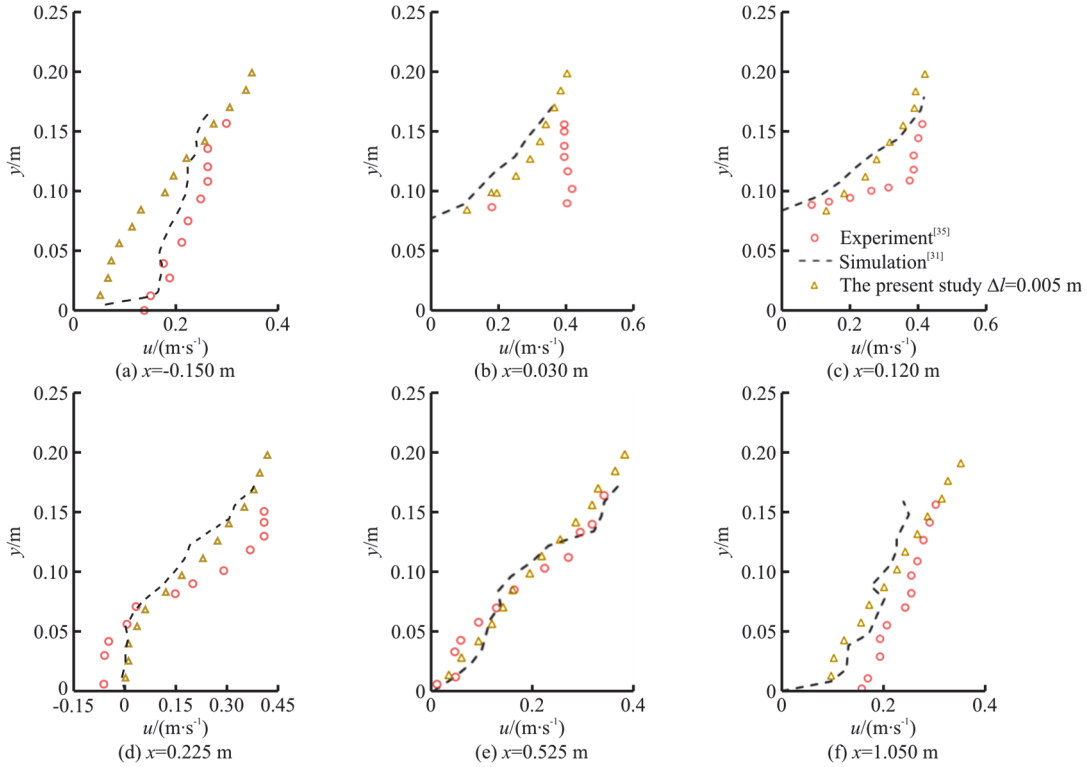

Fig. 12 (Color online) Comparison of horizontal velocity at different vertical sections for the flow over an obstacle

shows a good agreement with the experimental measurements at the vertical sections in the flow.

By simulating the three types of open channel flows, the explicit mesh-free method is shown to be able to reproduce the flow pattern and velocity information in the flows. On the other hand, there are some discrepancies in the velocity comparison. More accurate and high-order spatial models can improve the accuracy to simulate the open channel flows. The numerical scheme can also be enhanced by incorporating other turbulence models such as the k-ε model and robust numerical techniques in the mesh-free method.

Acknowledgements

This work was supported by the Key Research and Development Program of Zhejiang Province (Grant No. 2020C03082), the Visiting Researcher Fund Program of State Key Laboratory of Water Resources and Hydropower Engineering Science, Wuhan University (Grant No. 2021HLG01).

Compliance with ethical standards

Conflict of interest: The authors declare that they have no conflict of interest. David Z. Zhu is an editorial board member for the Journal of Hydrodynamics and was not involved in the editorial review, or the decision to publish this article. All authors declare that there are no other competing interests.

Ethical approval: This article does not contain any studies with human participants or animals performed by any of the authors.

Informed consent: Informed consent was obtained from all individual participants included in the study.

References

[1] Ye T., Pan D., Huang C. et al. Smoothed particle hydrodynamics (SPH) for complex fluid flows: Recent developments in methodology and applications [J]. *Physics of Fluids*, 2019, 31(1): 011301.

[2] Khayyer A., Shimizu Y., Gotoh H. et al. Multi-resolution ISPH-SPH for accurate and efficient simulation of hydroelastic fluid-structure interactions in ocean engineering [J]. *Ocean Engineering*, 2021, 226: 108652.

[3] Koshizuka S., Nobe A., Oka Y. Numerical analysis of breaking waves using the moving particle semi-implicit method [J]. *International Journal for Numerical Methods in Fluids*, 1998, 26(7): 751-769.

[4] Duan G., Chen B., Zhang X. et al. A multiphase MPS solver for modeling multi-fluid interaction with free surface and its application in oil spill [J]. *Computer Methods in Applied Mechanics and Engineering*, 2017, 320: 133-161.

[5] Xu T., Jin Y. C. Two-dimensional continuum modelling granular column collapse by non-local peridynamics in a mesh-free method with μ(I) rheology [J]. *Journal of Fluid*

Mechanics, 2021, 917: A51
[6] Sarkhosh P., Jin Y. C. MPS modeling of cross-sectional averaged shallow water flows with open boundaries using TVD-MacCormack predictor-corrector [J]. *Journal of Hydrology*, 2022, 608: 127566.
[7] Wen X., Zhao W., Wan D. A multiphase MPS method for bubbly flows with complex interfaces [J]. *Ocean Engineering*, 2021, 238: 109743.
[8] Lyu H. G., Sun P. N. Further enhancement of the particle shifting technique: Towards better volume conservation and particle distribution in SPH simulations of violent free-surface flows [J]. *Applied Mathematical Modelling*, 2022, 101: 214-238.
[9] Zhang Z. L., Khalid M. S. U., Long T. et al. Improved element-particle coupling strategy with δ-SPH and particle shifting for modeling sloshing with rigid or deformable structures [J]. *Applied Ocean Research*, 2021, 114: 102774.
[10] Khayyer A., Shimizu Y., Gotoh H. et al. Multi-resolution ISPH-SPH for accurate and efficient simulation of hydroelastic fluid-structure interactions in ocean engineering [J]. *Ocean Engineering*, 2021, 226: 108652.
[11] Zhang G., Zhao W., Wan D. Partitioned MPS-FEM method for free-surface flows interacting with deformable structures [J]. *Applied Ocean Research*, 2021, 114: 102775.
[12] Bui H. H., Nguyen G. D. Smoothed particle hydrodynamics (SPH) and its applications in geomechanics: From solid fracture to granular behaviour and multiphase flows in porous media [J]. *Computers and Geotechnics*, 2021, 138: 104315.
[13] Antuono M., Sun P. N., Marrone S. et al. The δ-ALE-SPH model: An arbitrary Lagrangian-Eulerian framework for the δ-SPH model with particle shifting technique [J]. *Computers and Fluids*, 2021, 216: 104806.
[14] Monaghan J. J. Smoothed particle hydrodynamics and its diverse applications [J]. *Annual Review of Fluid Mechanics*, 2012, 44: 323-346.
[15] Sun P. N., Luo M., Le Touzé D. et al. The suction effect during freak wave slamming on a fixed platform deck: Smoothed particle hydrodynamics simulation and experimental study [J]. *Physics of Fluids,* 2019, 31(11): 117108.
[16] Xu T., Jin Y. C. Numerical investigation of flow in pool-and-weir fishways using a meshless particle method [J]. *Journal of Hydraulic Research*, 2014, 52(6): 849-861.
[17] Khayyer A., Gotoh H., Shimizu Y. A projection-based particle method with optimized particle shifting for multiphase flows with large density ratios and discontinuous density fields [J]. *Computers and Fluids,* 2019, 179: 356-371.
[18] Tamai T., Koshizuka S. Least squares moving particle semi-implicit method [J]. *Computational Particle Mechanics,* 2014, 1(3): 277-305.
[19] Xu T., Jin Y. C. Improvement of a projection-based particle method in free-surface flows by improved Laplacian model and stabilization techniques [J]. *Computers and Fluids*, 2019, 191: 104235.
[20] Morikawa D., Senadheera H., Asai M. Explicit incompressible smoothed particle hydrodynamics in a multi-GPU environment for large-scale simulations [J]. *Computational Particle Mechanics*, 2021, 8(3): 493-510.
[21] Daly E., Grimaldi S., Bui H. H. Explicit incompressible SPH algorithm for free-surface flow modelling: A comparison with weakly compressible schemes [J]. *Advances in Water Resources,* 2016, 97: 156-167.
[22] Xu T. Explicit calculation for the pressure Poisson equation to simulate incompressible fluid flows in a mesh-free method [J]. *International Journal for Numerical Methods in Fluids*, 2021, 93(10): 3034-3052.
[23] Ye Y., Xu T., Zhu D. Z. Numerical analysis of dam-break waves propagating over dry and wet beds by the mesh-free method [J]. *Ocean Engineering*, 2020, 217: 107969.
[24] Zuo J., Xu T., Zhu D. Z. et al. Impact pressure of dam-break waves on a vertical wall with various downstream conditions by an explicit mesh-free method [J]. *Ocean Engineering*, 2022, 256: 111569.
[25] Xiao H., Jin Y. C. Development of explicit moving particle simulation method with applications [J]. *Computers and Fluids*, 2022, 235: 105270.
[26] Xu T., Jin Y. C. Numerical study of the flow over broad-crested weirs by a mesh-free method [J]. *Journal of Irrigation and Drainage Engineering*, 2017, 143(9): 04017034.
[27] Shao S., Gotoh H. Turbulence particle models for tracking free surfaces [J]. *Journal of Hydraulic Research*, 2005, 43(3): 276-289.
[28] Xu T., Jin Y. C. Improvements for accuracy and stability in a weakly-compressible particle method [J]. *Computers and Fluids*, 2016, 137: 1-14.
[29] Xu T., Jin Y. C. Simulation the convective mixing of CO_2 in geological formations with a meshless model [J]. *Chemical Engineering Science*, 2018, 192: 187-198.
[30] Khayyer A., Gotoh H. A 3D higher order Laplacian model for enhancement and stabilization of pressure calculation in 3D MPS-based simulations [J]. *Applied Ocean Research*, 2012, 37: 120-126.
[31] Fu L., Jin Y. C. A mesh-free method boundary condition technique in open channel flow simulation [J]. *Journal of Hydraulic Research*, 2013, 51(2): 174-185.
[32] Kirkgoz M. S., Akoz M. S., Oner A. A. Experimental and theoretical analyses of two-dimensional flows upstream of broad-crested weirs [J]. *Canadian Journal of Civil Engineering*, 2008, 35(9): 975-986.
[33] Xin Y. Flow characteristics in free and forced hydraulic jumps [J]. Brunswick, Germany: Technical University of Brunswick, Communication No. 119, 1993(in German).
[34] Liu Q., Drewes U. Turbulence characteristics in free and forced hydraulic jumps [J]. *Journal of Hydraulic Research*, 1994, 32(6): 877-898.
[35] Leu J. M., Chan H. C., Chu M. S. Comparison of turbulent flow over solid and porous structures mounted on the bottom of a rectangular channel [J]. *Flow Measurement and Instrumentation*, 2008, 19(6): 331-337.